TRANSITION EXPERIMENT WITH A BLUNT APOLLO SHAPE LIKE CAPSULE IN HYPERSONIC LUDWIEG TUBE

S.R.C. Ali*,
R. Radespiel*
*Institute of Fluid Mechanics, Technische Universität Braunschweig, 38108, Germany
A. Theiss‡;
‡German Aerospace Center, Institute of Aerodynamics and Flow Technology, Göttingen, 37073, Germany

Summary

Experimental and numerical results on laminar-turbulent transition in the boundary layer of a blunt Apollo-like capsule at 0◦ and 24◦ angle of attack (AOA) are presented. Infrared thermography was used to observe the transition behavior for varying unit Reynolds number runs (Re_∞ = 6e6 /m to Re_∞ = 20e6 /m) and for two different surface condition. For the investigated capsule surface with a mean roughness of R_a = 10 µm, transitional surface heating firstly appeared at about Re_∞ = 15e6, whereas for a mean roughness of R_a = 0.5 µm no indications for a transitional boundary layer were found at all. PCB and Kulite sensors are used to measure surface pressure fluctuations inside the boundary layer, but did not show any peaks in the frequency spectra which might be related to harmonic boundary layer disturbances. The only relevant peak in the spectra is attributed to bow shock oscillations. Space/time correlations of pressure data indicates low linear correlation of consecutive and crosswise placed sensors and help to characterize the nature of pressure fluctuation.

1. MOTIVATION

Manned space transportation relies entirely on capsules, in the post US-Shuttle era. Currently, the exploration spacecraft Orion is in the design and construction process for manned mission to moon and mars. One part of the vehicle, the Apollo shape like service module capsule, will be equipped with a blunt heat shield system. The size of the thermal protection shield is estimated by the turbulent boundary layer. Over a wide range along the projected return path the flow remains laminar before it transitions to turbulence. The heat flux in the laminar case can locally be much less than the turbulent flux, which under current design assumptions leads to an over-dimensioning of the heat shield. Additionally to the transition mechanism on the front surface of the capsule, efforts are needed to analyze transition to turbulent flow in the aftbody region, where reattached turbulent flow can increase heating, leading to significant amounts of local fluxes compared to stagnation point heating [1]. For future reentry space vehicles all flow regimes and all parts of the capsule which are exposed to aerodynamic heating have to be considered and a reliable prediction of the transition onset location needs to be known. Until now transition onset location on capsules has been correlated to some integral boundary layer values such as Reynolds number based on displacement or momentum thickness. A more physically based method is the stability analysis, where the disturbance growth in the laminar base flow is investigated. So far stability analyses have only been made public in the design phase of the Mars Science Laboratory, where transition was dominated by 1st mode and cross-flow instabilities [2, 3]. A detailed overview of wind tunnel measurements on the mentioned capsule shapes, with empirical correlations for transition onset, is given by Hollis [4]. Instability mechanisms of hypersonic flow over blunt capsules leading to transition may arise from several sources. One of them is out-gassing from an ablative heat shield. Li et al. [5] demonstrated the destabilizing effect of ablation induced out-gassing on a boundary flow over a hemispherical capsule which otherwise did not support amplification of instability modes. Other transition initiating sources, among others, are surface distributed roughness or roughness-induced transition behind a discrete roughness element. Amar et al.[6] demonstrated the effect of isolated protuberances on the laminar to turbulent transition on the CEV capsule in wind tunnel experiments, whereas Hollis [7] validated the influence of distributed roughness effects on the blunt-body transition. An extensive summary on roughness related transition in hypersonic boundary layers on blunt bodies is given by Schneider [8]. In the present paper the ongoing work of a German cooperative research project on a blunt generic re-entry capsule is reported. Results of transition experiments on a generic Apollo capsule model carried out in Hypersonic Ludwig tube Braunschweig (HLB) are presented. For measuring transition onset location infrared thermography is used. The capsule model is equipped with surface mounted high-frequency pressure sensors to discover boundary layer modes. In order to examine surface roughness effects, two different surface finishes have been used with a mean roughness of R_a = 0.5 and 10 µm.

2. EXPERIMENTAL SETUP

2.1. Windtunnel

The experiments were conducted in the hypersonic Ludwieg tube (HLB) at the Technische Universität Braunschweig. This is a blow down tunnel which was previously qualified and calibrated by Estorf et al. [9]. The assembly is divided into two pressure regions, according to figure 1. One is the pressurized storage tube (4-30 bar), subdivided into a cold and a heated part (up to 500 K) to

prevent condensation effects during the expansion in the nozzle. The heated section accommodates the amount of gas that is released during one run. The low-pressure wind tunnel parts are nozzle, test section and dump tank. These are evacuated prior to each run to <3 mbar. High and low pressure parts are separated by a pneumatically driven valve. After opening the valve the air is accelerated towards the test section. The Mach number in the test section is between 5.85-5.9 depending on the initial driver tube pressure and on the position in the test section. The flow conditions are steady for about 80 ms and the unit Reynolds number range is [3-30]·10e6/m. The unit Reynolds number is computed from the initial driver tube pressure and the temperature in the driver tube during the run (overall uncertainty about 2 %). The noise level is typical for a conventional facility and relative stagnation-probe pressure fluctuations range from 1-1.6 % [10]. More detailed measurements and analysis of the freestream disturbances are presented in a more recent paper [11].

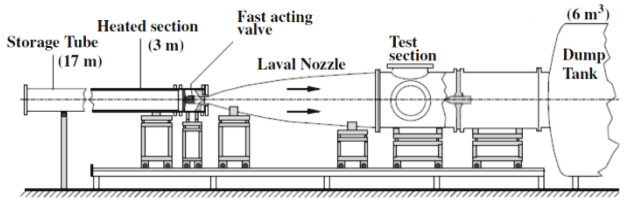

FIGURE 1: Sketch of the HLB facility of TU Braunschweig

2.2. Wind tunnel model

An Apollo capsule model was designed and built after preliminary tests of the maximum model size that can be run in the tunnel. These tests showed that the maximum model diameter is about 180 mm. To assure reliable wind tunnel operation at all flow conditions a size of 170 mm was chosen. Reliable wind tunnel operation was checked by taking Schlieren images and by scrutinizing the shape of the bow shock and its stand-off distance. Such Schlieren images for 0° and 24° AOA are depicted in figure 2 with overlaying Mach number isolines from corresponding CFD simulations. The model is made from black plexiglas (black 811-Röhm-GS). This material is painted with Nextel velvet coating, which exhibits a low transparency and high emissivity coefficient. This allows measuring the instantaneous transient surface temperature with a suited infrared camera. The infrared measurements were conducted to determine the heat flux and estimate the region of laminar-turbulent transition. The model is split into three parts to allow instrumentation with surface sensors, see figure 3. The front part is a single part to prevent surface inhomogeneities that might affect boundary layer transition. Also, to reduce roughness the surface was carefully polished. Some isolated roughness results from the nominally flush mounted sensors and the maximum value was measured as k_s = 0.039 mm. The influence of distributed roughness due to the coating was also investigated and results are given later. The sensor positions are indicated in the sketch of the model in figure 3. Most sensors are located along one line in radial direction. Several sensors are clustered in a group in order to conduct correlation measurements.

2.3. Instrumentation and data reduction

The instantaneous surface temperature was measured with a high-speed infrared camera of type ImageIR 8320 of the company InfraTec. The camera's InSB-chip is sensitive in the mid-IR range (2-5.7 µm) and has a resolution of 640x512 pixel^2.

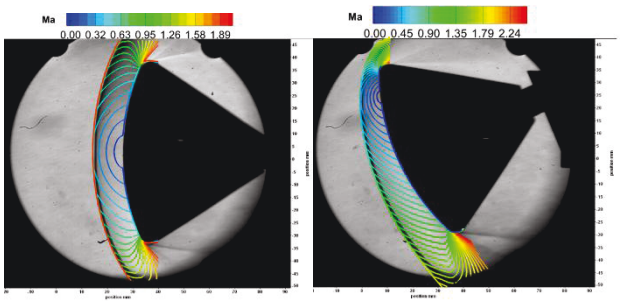

FIGURE 2: Schlieren images of Apollo capsule at 0° and 24° AOA with overlaying Mach number isolines from a CFD simulation

The maximum frame rate at full resolution is 100 Hz, which was used for the present IR-measurements. For the data analysis an in-house heat flux calculation program was used. This is described in detail in Estorf [12] and Estorf [13]. It consists of temperature calibration, spatial calibration and different algorithms to compute the heat fluxes from the temperature data. For the results reported here lateral heat fluxes within the model are neglected. The heat conduction equation is solved numerically using finite differences. The unknown heat flux is found by an iterative regularization method. Here the surface temperature calculated from an iteratively improved heat flux is compared to the measured values in a least-squares formulation. The gradient for iterative correction of the heat flux is found by solving the adjoint problem. The stopping criterion is adjusted to the noise level of the measured temperature data. During one tunnel run 8-11 images were taken and the just mentioned procedure was applied. Then, averages of the heat flux obtained from the data at several time instances are taken to reduce noise. Furthermore, to detect fluctuations in the boundary layer the capsule front was instrumented with different high-frequency pressure sensors. These were nine PCB M132A31 pressure fluctuation sensors and two Kulite

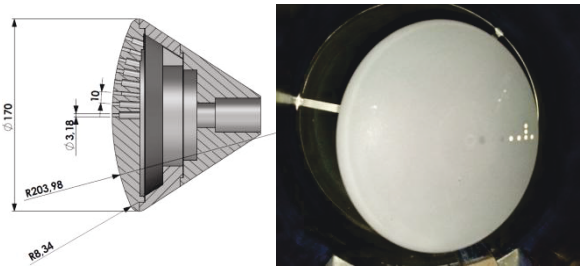

FIGURE 3: Left: Sketch of the Apollo capsule model. Right: Front surface of instrumented and coated capsule model

XCS062 sensors. The PCB sensors have been widely used in the last years for measurements of super and hypersonic boundary layer instabilities. Although the boundary layer for this blunt geometry is rather thin (and therefore any boundary layer instabilities would exhibit rather short wavelengths) we tried these sensors due to the good experiences gained in the past years [14]. The sensors have a diameter of 3.18 mm. However, the active area has a rectangular shape of 0.8 x 0.8 mm^2. The resonance frequency as specified by the manufacturer is above 1 MHz. Power was supplied using a M483A instrument which also performed signal conditioning. This includes a high-pass filter at 11 kHz. The Kulite sensors have resonance frequencies of 200 kHz. Thus they are suited for the measurement of the mean pressure and of fluctuations up to about 50 kHz. This is assumed high enough to capture the relevant disturbance frequencies in the boundary layer of the blunt Apollo geometry. The purpose of these sensors is to gain data in the frequency range below 11 kHz, where the PCB signal is not reliable. The data of both pressure sensors were sampled with a M2i.4652 transient recorder (company Spectrum) with a sampling frequency of 3MHz in 16 bit format. The acquired time traces were used to compute disturbance spectra. Therefore the signal was divided into windows of 2048 data points. Each window was multiplied with a normalized Blackman window and Fourier transformed. Then the average of these windows was taken. Also a spectrum from the time prior to the run was computed and this was subtracted from the spectrum during the tunnel run time in order to reduce the electric noise of the measurement chain. With the chosen Fourier transform parameters the frequency resolution is Δf = 1.46 kHz.

3. RESULTS

3.1. Heat flux measurements

In this section the measured heat flux data are compared to results from numerical computations. Measurements were conducted with standard black coating and with a highly polished surface without coating, in order to assess a possible effect of surface roughness. For both cases the surface roughness was measured. With standard coating the mean roughness is R_a = 10 µm, whereas for the highly polished model a mean roughness of R_a = 0.5 µm was measured.

3.1.1. Standard coating

Figure (4) and (6) depict a comparison of computed and measured heat flux for the capsule at an angle of attack of 24°, for different Reynolds numbers. Here the IR coating (R_a = 10 µm) was used. For the lower unit Reynolds number the agreement appears to be good, as the boundary layer is laminar over the entire blunt side of the capsule. The heat flux decreases towards the capsule shoulder on the lee side by a factor of about two. In the direct vicinity of the shoulder it increases again. Here the boundary layer is affected by the strong expansion resulting in a decreasing boundary layer thickness and higher heating loads. Detailed analysis of the results show that the computation resolves the flow phenomena very well and that the boundary layer in the experiments at low Reynolds number is fully laminar. Around the stagnation point a locally larger heating is observed in the measurement. Such a stagnation point heat flux augmentation was already reported in the literature, e.g. in Ref. [15]. At the higher unit Reynolds number the experimental heat flux indicates a transitional boundary layer over parts of the surface. Therefore the agreement to the fully laminar computation is not as good. The stagnation point exhibits a stronger heating in this case. Towards the lee-side the heat flux decreases at first, then it gradually increases again indicating the onset of transition. The area of large heating occurs in a moon shape, involving the stagnation point heating. This particular transition shape is at the moment believed to be affected by the increased fluctuations of the wake flow of the wind tunnel piston which is located at the central axes. This sensitivity of heat flux augmentation on the model position in the test section needs to be further investigated. For the figures (5) and (7) the heat flux data were extracted along the symmetry plane of the capsule. Here the coordinate x represents the projection of the surface arc length onto the yz-plane. The origin x = 0 mm is set at the intersection point of capsule shoulder and capsule front. The heat flux in figures (5) and (7) is presented in non-dimensional form as Stanton number. Both cases show similar differences in the heating rates, as the measured heating rate is larger compared to the numerical simulation over a significant portion of the windward surface. It appears that heating rate augmentation in the stagnation region is around 30% for the smaller Reynolds number. Part of this may be due to surface roughness as will be shown below. For Re_∞ = 18e6 /m the deviation between measured and computed heat flux in the stagnation region is smaller. However, an increase in the measured heat flux of the leeward surface region is visible (starting from x = 110 mm). This case appears to be transitional although the Reynolds number is not large enough to yield fully turbulent flow.

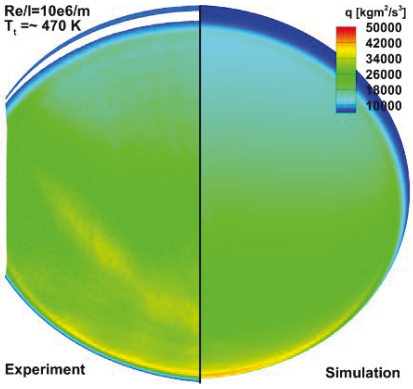

FIGURE 4: Contours of experimental and computed heat flux for Re/l = 10e6 /m, R_a = 10 µm

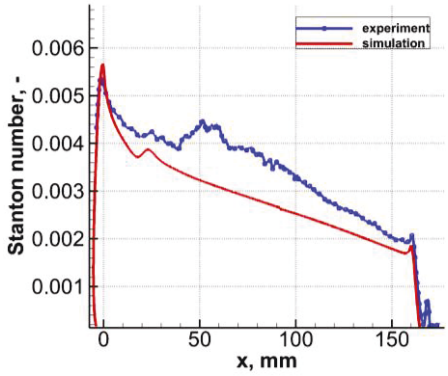

FIGURE 5: A quantitative comparison in the symmetry plane of experimental and computed heat flux for Re/l 10e6 /m, R_a = 10 µm

The observed sensitivity of stagnation heat flux augmentation with respect to the Reynolds number comparison differs from the results in Ref. [15]. We note that leeside transition for the coated capsule begins at a freestream unit Reynolds number of Re/l = 16e6/m which can be observed from figure (8).

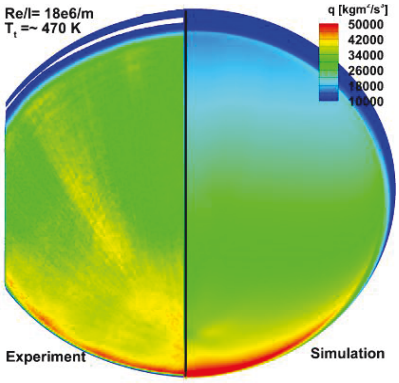

FIGURE 6: Contours of experimental and computed heat flux for Re/l = 18e6 /m, R_a = 10 µm

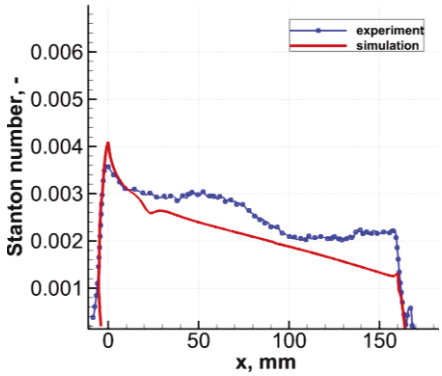

FIGURE 7: A quantitative comparison in the symmetry plane of experimental and computed heat flux for Re/l = 18e6 /m, R_a = 10 µm

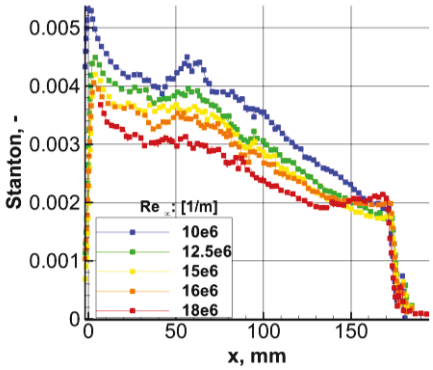

FIGURE 8: Stanton number distribution in the symmetry plane for different unit Reynolds numbers, Ra = 10 µm

3.1.2. Highly polished capsule

For the measurements reported in the following the coating was removed and the surface was highly polished. Hence, the remaining mean roughness was much smaller, R_a = 0.5 µm. In this case the largest local roughness was due to the sensors. The effect of the sensor roughness was removed by rotating the model, so that the sensors did not disturb the IR-data. The evaluation of the surface heat flux from the infrared data does not result in accurate absolute results since plexiglas has a significantly larger transparency to infrared radiation compared to the coating. Hence a temperature slightly inside the model rather than the surface temperature is measured [13]. Therefore, the heat flux data from the model without coating was made non-dimensional using the stagnation point heating as a reference.

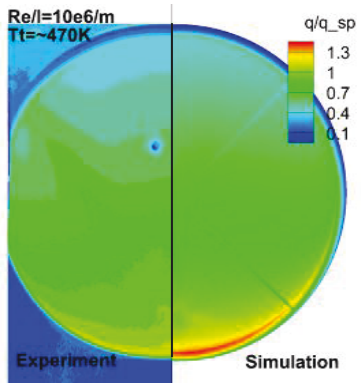

FIGURE 9: Contours of experimental and computed heat flux for Re/l = 10e6 /m, R_a = 0,5 µm

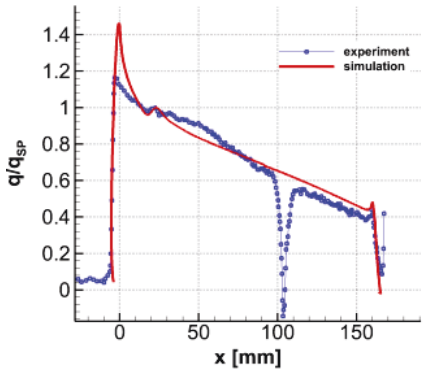

FIGURE 10: Quantitative comparison in the symmetry plane of experimental and computed heat flux for Re/l = 10e6 /m, R_a = 0.5 µm

Figure (9) and (10) show the comparison between experimental and computed heating rates for the polished surface, at the lower Reynolds number. The agreement of experimental and numerical data for the polished surface is much better than for the model with coated surface. Here, three noteworthy differences between measured and computed heat flux must be mentioned. The measurement displays a strong spike at x = 104 mm. This can be seen in both plots and shows the reflection of heat radiation emitted from the hot piston in the center of the wind tunnel throat. Secondly, the heating rates at the windward capsule shoulder are smaller than predicted by the computation, most probably due to the small angle under which the camera sees this part of the surface. And thirdly, the region of locally increased heat flux near the stagnation point seems to be somewhat larger in the experiment compared to the computation. The comparison between the heat fluxes of the coated and polished models indicates that stagnation heating augmentation is related to surface roughness.

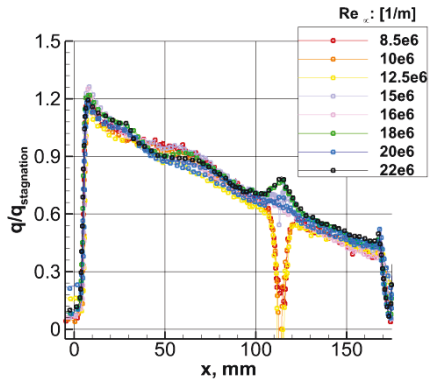

FIGURE 11: Non-dimensional experimental heat flux in the symmetry plane for different unit Reynolds numbers, highly polished capsule, R_a = 0.5 µm

With the polished model a Reynolds number variation was also conducted and the results are given in figure (11). The heat flux in the symmetry plane is presented for a unit Reynolds number range, Re/l = [8.5 - 22] e6/m. In this case the boundary layer does not show significant signs of transition to turbulence. Instead all data lines collapse rather well and they all show a decrease in heating by a factor of two towards the leeward capsule shoulder.

3.2. Surface pressure data

3.2.1. Dynamic pressure response

The capsule forebody was instrumented with several high-frequency pressure sensors in order to capture possible boundary layer instabilities. These measurements were conducted with the coated model (R_a = 10 µm) for 0°, 24° angle of attack and rotated sensor position. The color coded infrared image in figure (12) depicts the different sensor positions. The image indicates that the roughness due to the instrumentation has a critical height to trigger transition of the boundary layer for runs at high unit Reynolds number. Sensor position 5 denotes the location closest to the stagnation point and position 0 refers to the sensor closest to the capsule shoulder. Both sensors are located 30 mm apart. In figure (13), spectra for a high unit Reynolds number run and for 0° and 24° angle of attack are presented. It is seen that the 0° case shows higher dynamic pressure fluctuations for the entire frequency range compared to the 24° configuration. This may be due to the fact that shock strength around the sensor position is stronger at 0°. One also observes a small bump of the spectrum at about 25-50 kHz for 0° which is more visible for the 24 degree setup. It appears that this peak is insensitive to changes in Reynolds number. As the boundary layer thickness is very low at 0° [16], the idea to observe the model at an angle of attack of 24° is to obtain larger variations of boundary layer thickness over the capsule. Figure (14) displays disturbance spectra from the PCB sensors at two positions for three different Reynolds numbers. These spectra collapse to a single line for both positions. With increasing Reynolds number the amplitudes slightly increase. For position 5 the relevant low-frequency peak is more pronounced than for position 0. At this point we interpret this peak as an indication of a sound wave that is trapped between model surface and bow shock. Such an acoustic wave might emanate from fluctuations of the shock, e.g. as consequence of free stream disturbances or particle impacts. The frequency can be estimated from twice the shock stand-off distance and the speed of sound between shock and model. This frequency estimate roughly corresponds to the peak in the spectra. It seems that there are no peaks related to effects inside the boundary layer. This observation may also be due to the size of the sensor. Consistent with the experimental findings, the modal instability analysis does also not provide any modal boundary layer disturbance growth at wind tunnel conditions [16]. We also notice from figure (11) that at the high Reynolds number Re/l=18e6/m the sensors at positions 0 and 5 are located in very different surface flow regions, i.e. sensor 0 is located in the turbulent wake of the upstream sensors. Nevertheless, this does not result in significant changes in the frequency response. That means one cannot distinguish between laminar and turbulent pressure fluctuation spectra. In consequence, this leads to conclusion that measurement of dynamic surface pressure alone is not sufficient to characterize heat flux rise due to transition process in an accelerated boundary layer of a blunt capsule. Note that Marineau [15] characterized heat flux and pressure fluctuations in augmented laminar blunt

body heating by determining the lengths scale out of space time correlation of the temperature and heat flux data obtained from ALTP and thermocouple sensors. This strategy will be applied using pressure data and presented in subchapter 3.2.2

Next, figure (15) displays a spectrum of a Kulite sensor which is located at the same radial position as the PCB at position 5. These sensors are more reliable in the low frequency range (below 11 kHz). Moreover, their membrane is smaller than the active area of the PCBs as these sensors have a diameter of only 1.7 mm. Therefore the spatial averaging might be smaller than in the case of the PCBs. However, the disturbance spectra in figure (15) of these sensors only show a single peak at 25-50 kHz. Note that at frequencies above 50 kHz the dynamic response of the Kulite is affected by the limited resolution due to resonance. The measured peak is consistent with the PCB data and so far we interpret these bumps in the pressure fluctuation as result of a bow shock oscillation.

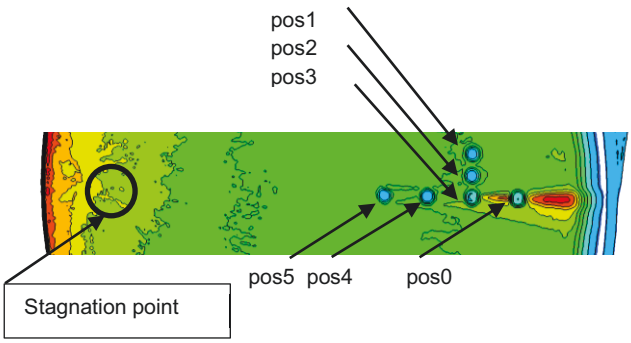

FIGURE 12: Sensor positions on the capsule (contour plot of heat flux at Re/l=18e6/m)

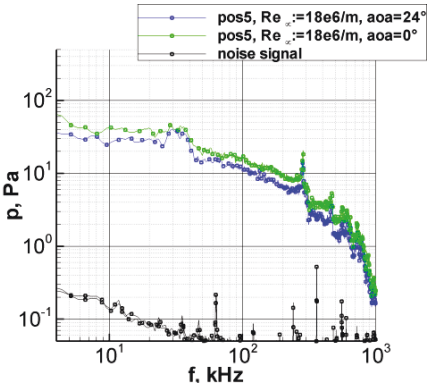

FIGURE 13: Disturbance spectra of two pressure signals obtained at two different AoA

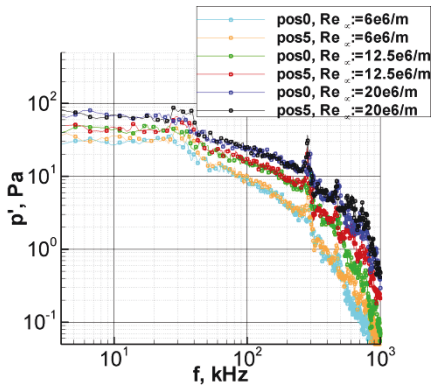

FIGURE 14: Disturbance spectra based on PCB measurements for two measurement positions at three different unit Reynolds numbers

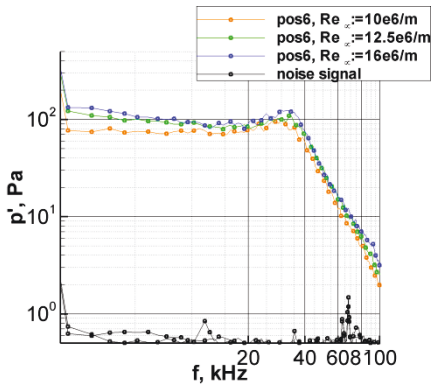

FIGURE 15: Disturbance spectra based on measurements with Kulite xcs062 for three unit Reynolds numbers

3.2.2. Correlation analysis

For further analysis the recorded dynamic surface pressure readings from the PCB sensors were scanned with space-time cross and auto correlations to investigate any hints of detectable disturbance structures, thereby providing further characterization measured fluctuations. To improve signal quality the raw data were band-pass filtered for certain frequency bandwidth where the spectral distribution of the pressure shows some recognizable peaks. One is the previously discussed peak in range of 25-50 kHz. For its analysis the sensors where aligned in streamwise direction. The content of the pressure rise above 280 kHz is assumed to depend on the measurement chain. It does only show correlation values below 0.2 and these results are not shown here.

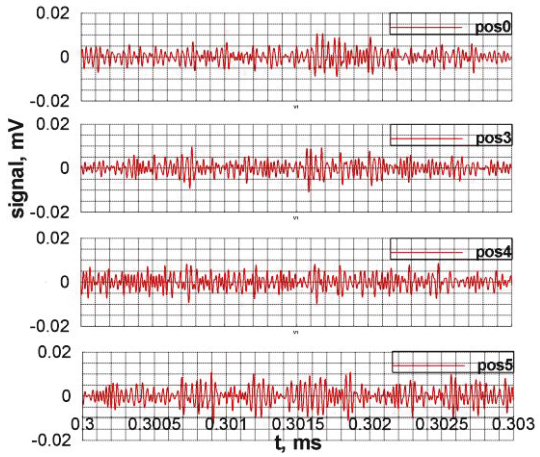

FIGURE 16:Filtered (20-50Khz) time traces of consecutive pressure sensors, Re/l=18e6/m

As presented in figure (16) the filtered time traces do not provide indications of moving structures at first sight. Then, figure (17) displays the applied space time correlation between pairs of sensors in streamline direction. A weak linear correlation between the sensors is visible for the unit Reynolds number of 10e6/m (laminar flow over the whole capsule) where the highest correlation coefficient is found for the most downstream sensor pair (pos3pos0).

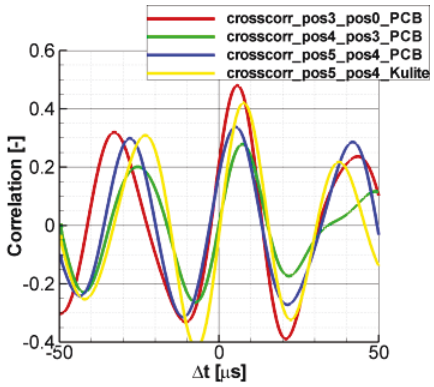

FIGURE 17: Consecutive pressure sensors and result of cross-correlation for sensors on same streamline, Re/l=10e6/m.

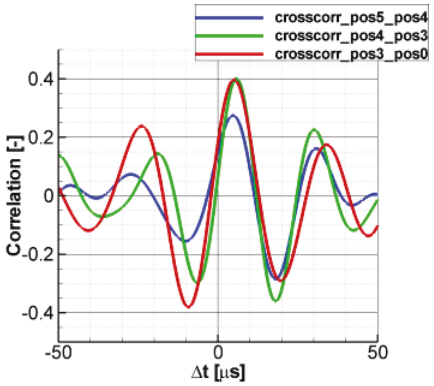

FIGURE 18: Consecutive pressure sensors and result of cross-correlation for sensors on same streamline, Re/l=18e6/m.

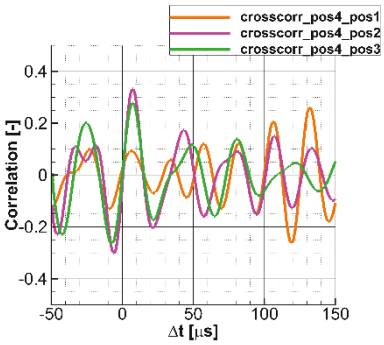

FIGURE 19: Diagonally placed pressure sensors and result of cross-correlation, Re/l=10e6/m.

The correlation peaks decrease away from their maximum, except for sensor position 5 and 4 where pressure fluctuations correlate periodically, at the same level. A quite good agreement with these findings was observed in the correlation of the Kulite readings (not shown). Comparing figure 17 with the results in figure 18 obtained for a higher unit Reynolds number (18e6/m) where the data was already affected by transition process, one can see that the correlation peaks are more compressed than before. This may indicate that the flow structure that corresponds to the pressure fluctuation propagating downstream, changes its lengths scale and is unit Reynolds number dependent, similarly as observed in the work of Marineau [15]. Further one can note that both, the low Reynolds number (10e6/m, laminar flow) and the high Reynolds number (18e6/m, partly transitional) correlations show alternating correlation, similar to the findings of low-frequency pressure correlation measured by Beresh [17]. Note that opposed to Beresh's results the present results suggest that anti-correlation are the typical signature of turbulent pressure fluctuations. Our investigation of spanwise propagation of pressure fluctuations is illustrated in figure (19). Therefore, a signal is obtained at sensor 4 and this signal is correlated with downstream sensors that are displaced in spanwise direction. It is noticed that the correlation between two closest sensors exhibit the maximum value. Additionally, significant correlation values are observed for spanwisely staggered sensors that go along with a shift in time. It appears that pressure fluctuations also propagate perpendicular to the streamline direction.

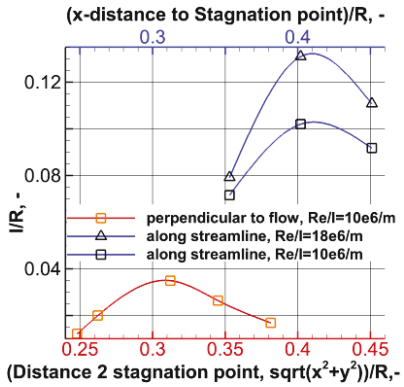

FIGURE 20: Calculated and normalized length scales

In contrast to Marineau's determination of length scales out of the heat flux and temperature signals obtained on a 7 inch model, the lengths scales presented in figure (20) are here based on the bandpass filtered surface pressure. We note that Marineau's investigations were carried out for higher Mach number of 9 and a larger range of unit Reynolds numbers, [1.5-80] 10e6/m. The presented lengths scales were calculated with the integral time as the distance between correlation peak and time shift of zero and simply multiplied with the boundary layer edge velocity obtained from the computation [16] in position in-between to sensor locations. The results are shown in figure (20), where two groups of normalized lengths scales as a function of normalized distance to the stagnation point are illustrated. One realizes that the relative lengths scales of pressure fluctuations in streamline direction are bigger than for perpendicular propagating pressure fluctuations. We note that length scale due to perpendicular propagation was not found in [15] as only temperature fluctuations were measured. One also observes that measured length scale grows with the Reynolds number. And finally, one can observe for both lengths scales that they grow until a certain distance and then decreases to smaller values. As the pressure fluctuation follows somehow the flow, this behavior could be caused by some curvature effects which lead to partly diffracted pressure fluctuations.

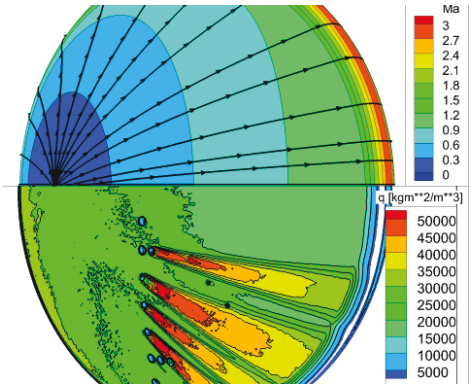

FIGURE 21: Sensor positions on the capsule for rotated configuration (contour plot of heat flux at Re/l=18e6/m). Upper part: Illustration of streamlines

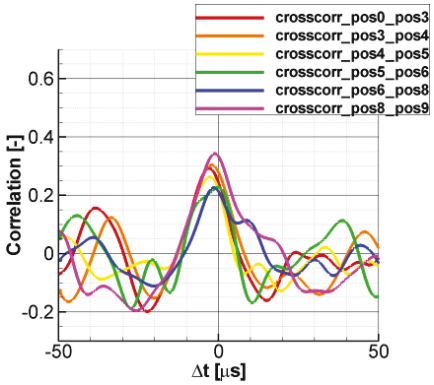

FIGURE 22: Perpendicular placed pressure sensors and result of group wise cross-correlation, Re/l=10e6/m,

In a rotated capsule configuration, the pressure sensors are mounted perpendicular to the flow direction as shown in figure (21). In this configuration the analyzed groups of sensors are no more aligned to streamlines, see upper side of figure (21). The heat flux contour plot also indicates which sensors initiated boundary layer transition and illustrate the streamlines for an adjusted capsule model at 24° AOA. Anyway, the correlation analysis reveals a weak interrelation with a coefficient of nearly 0.3 between the pressure data which were measured 10 mm apart (figure 22). This result may help to better understand the behavior of the pressure fluctuations. The main propagation direction is aligned with the streamline but also crosswise propagation of pressure fluctuations could be seen.

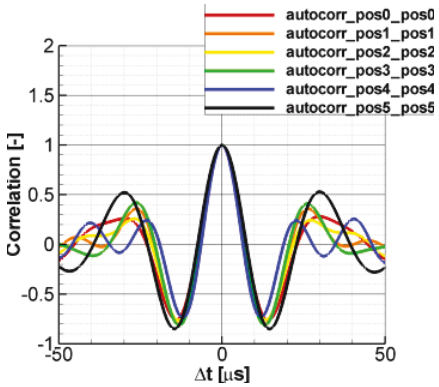

FIGURE 23: Autocorrelation of band-pass filtered pressure data at Re/l=10e6/m

The autocorrelation displayed in figure (23) is often being used to calculate the lengths scales of coherent disturbance structures in streamwise direction by assuming that the convective velocity is the same as boundary layer edge velocity [17]. Following this assumption and using twice the time interval of the first intersection point multiplied with the convected velocity over the specific sensor position for computing the integral time scale, the characteristic length scale can be computed (results are not shown here). We note that the non-linear and non-stationary pressure data needs to be further investigated. A promising method could be the Hilbert-Huang Transformation e.g. in particular the intrinsic mode functions which allow separating the fluctuation values and relate them to certain frequency bandwidth. In additionan, any possible mode-mixing can be prohibited in that approach.

4. FUTURE WORK

So far experimental data has shown significant effect of mean surface roughness heights R_a on laminar to turbulent transition process on a blunt Apollo-like capsule. In a next step the wake flow behind discrete roughness elements in shape of cylinder and diamond elements will be investigated. Measurements will be carried out in the HLB with a segmented capsule with an outer rotating part to measure pressure as well as heat flux fluctuations. We hope to identify vortical structures by correlations form carefully staggered sensors. Simultaneously, simulations will be performed to characterize the wake of critical isolated roughness elements. In figure (24) the design of

the segmented capsule model is illustrated.

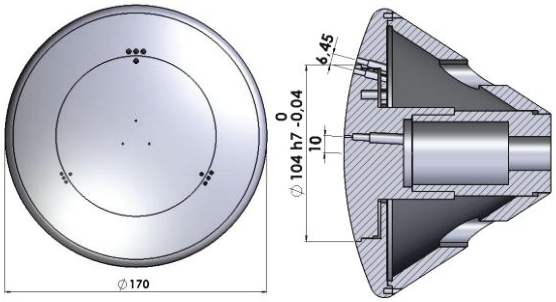

FIGURE 24: Sketch of the segmented model

5. CONCLUSION

Heat transfer and pressure measurements were conducted for the Apollo-like geometry in the Hypersonic Ludwieg Tube Braunschweig that corresponds to extensive numerical simulations [16]. Infrared thermography has been used to detect boundary layer transition and surface mounted high-frequency pressure sensors were implemented to discover possible boundary layer instabilities. The boundary layer on such a blunt geometry is extremely thin. Taking that into account the influence of surface roughness was also investigated by using the model with a typically used coating with high emissivity and a highly polished surface without coating. While for the model with standard coating the boundary layer was transitional near the leeward capsule shoulder for sufficiently high Reynolds number (>15e6/m), it was fully laminar in the case of improved finish quality. In the case of highly polished surface the agreement to the numerically simulated heat flux was found to be very good, while for the rougher surface deviations of up to 30% were observed. The pressure sensors did not show any modal instability waves which are consistent to the result of stability computations of Theiss [16]. A more detailed analysis of high frequency pressure data was performed for better understanding of the structure of flow fluctuations. These analyses identified the predominant main propagation direction.

REFERENCES

[1] Raper, R. M., “Heat-Transfer and Pressure Measurements Obtained During Launch and Reentry of the First Four Gemini-Titan Missions and Some Comparisons with Wind-Tunnel Data,” NASA Technical Memorandum TM-X-1407, Aug. 1967.

[2] Chang,C.-L.; Choudhari, M.; Hollis, B.R. and Li, F., Transition Analysis for the Mars Science Laboratory Entry Vehicle, 41st AIAA Thermophysics Conference, AIAA Paper 2009-4076, 2009.

[3] Johnson, H. B.; Candler, G. V.; Wright, M.J.,Boundary Layer Stability Analysis of Mars Science Laboratory Aeroshell, 44th AIAA Aerospace Sciences Meeting and Exhibit, AIAA 2006-920, Reno, Nevada, 09-12 January 2006.

[4] Hollis, B. R.,Blunt-Body Entry Vehicle Aerothermodynamics: Transition and Turbulence on the CEV and MSL Configurations, NASA Report No. NF1676L - 9838, 2010.

[5] Li, F.; Choudhari, M.; Chang, C.-L.; White, J., Boundary Layer Transition over Blunt Hypersonic Vehicles Including Effects of Ablation- Induced Out-Gassing, 6th AIAA Theoretical Fluid Mechanics Conference, AIAA Paper 2011-3303, 2011.

[6] Amar, A.J., Horvath, T.J., Hollis, B.R., Berger, K.T., Berry, S.A. and Calvert, N., Protuberance Boundary Layer Transition for Project Orion Crew Entry Vehicle, 46th AIAA Aerospace Sciences Meeting and Exhibit, AIAA Paper 2008-1227, 2008.

[7] Hollis, B. R., Distributed Roughness Effects on Blunt-Body Transition and Turbulent Heating, AIAA SciTech, 2nd Aerospace Sciences Meeting, AIAA Paper 2014-0238, 13 - 17 January 2014, National Harbor, Maryland.

[8] Schneider, S. P., Hypersonic Boundary-Layer Transition on Blunt Bodies with Roughness, 46th AIAA Aerospace Sciences Meeting and Exhibit, AIAA Paper 2008-501, 7 - 10 January 2008, Reno, Nevada.

[9] Estorf, M.; Wolf, T.; Radespiel, R., Experimental and numerical investigations on the operation of the hypersonic Ludwieg Tube Braunschweig. Proceedings 5th European Symposium on Aerothermodynamics for Space Vehicles, 8-11 November 2004, ESA SP-563, 2005, pp. 579- 586

[10] Heitmann, D.; Kähler, C.; Radespiel, R.; Rödiger, T.; Knauss, H. and E. Krämer., Disturbance-level and transition measurements in a conical boundary layer at Mach 6, 26th AIAA Aerodynamic Measurement Technology and Ground Testing Conference, AIAA Paper 2008-3951, 2008.

[11] Ali, S.R.C.; Radespiel. R.; Schilden, T.; Schröder, W, High-Frequency Measurements of Acoustic and Entropy Disturbances, 44th AIAA Fluid Dynamics Conference, AIAA-2014- 2644, Atlanta, 16-20 June 2014.

[12] Estorf. M., Image based heating rate calculation from thermographic data considering lateral heat conduction, Int. J Heat Mass Transfer, 49:2545-2556, 2006.

[13] Estorf, M., Ortsaufgelöste Bestimmung instationärer Wärmestromdichten in der Aerothermodynamik, ZLR-Forschungsbericht 2008-05, ISBN 978-3-8322-7195-4, Shaker Verlag, Aachen, 2008.

[14] Muñoz, F.; Heitmann, D.; Radespiel, R.S., Instability Modes in Boundary Layers of an Inclined Cone at Mach 6, 42nd AIAA Fluid Dynamics Conference and Exhibit, AIAA Paper 2012-2823, 25 - 28 June, New Orleans, Louisiana, 2012.

[15] Marineau, E. C.; Lewis, D. R.; Smith, M. S.; Lafferty, J. F., White, M. E., Amar, A. J., Investigation of Hypersonic Laminar Heating Augmentation in the Stagnation Region, 51st AIAA Aerospace Sciences Meeting, AIAA-2013-0308, Grapevine, Texas, 07-10 January 2013.

[16] Theiss, A.; Ali, S.R.C; Hein, S.; Heitmann, D.; Radespiel, R., Numerical and Experimental Investigation of Laminar-Turbulent Boundary Layer Transition on a Blunt Generic Re-entry Capsule, 44th AIAA Fluid Dynamics Conference, AIAA Paper 2014-2353, Atlanta, 16-20 June 2014-2353

[17] Beresh, S.J. et al, Very-large-scale coherent structures in the wall pressure field beneath a supersonic turbulent boundary layer, PHYSICS OF FLUIDS, 095104 (2013)